Applied Catalysis B: Environmental 99 (2010) 265–271

Contents lists available at ScienceDirect

Applied Catalysis B: Environmental

journal homepage: www.elsevier.com/locate/apcatb

Ethanol oxidation reactions using SnO_2@Pt/C as an electrocatalyst

J.C.M. Silva [a], R.F.B. De Souza [a], L.S. Parreira [a], E. Teixeira Neto [a], M.L. Calegaro [b], M.C. Santos [a,*]

[a] LEMN – Laboratório de Eletroquímica e Materiais Nanoestruturados, CCNH – Centro de Ciências Naturais e Humanas, UFABC – Universidade Federal do ABC, CEP 09.210-170, Rua Santa Adélia 166, Bairro Bangu, Santo André, SP, Brazil

[b] Grupo de Materiais Eletroquímicos e Métodos Eletroanalíticos–Instituto de Química de São Carlos, Universidade de São Paulo, Caixa Postal 780, 13566-590 São Carlos, SP, Brazil

ARTICLE INFO

Article history:
Received 11 November 2009
Received in revised form 11 June 2010
Accepted 18 June 2010
Available online 25 June 2010

Keywords:
Core–shell
SnO_2@Pt
PtSn/C
Ethanol oxidation reaction
Electrocatalysis

ABSTRACT

This paper presents a study on the ethanol oxidation reaction using SnO_2@Pt/C core–shell structures as electrocatalysts. All the materials used, including Pt/C and PtSn/C E-tek, were 20% (w/w) metal on carbon. The formation of core–shell nanoparticles (SnO_2@Pt/C) was measured by UV–vis spectrophotometry. X-ray diffraction measurements showed Pt (shell) diffraction patterns without influence from the SnO_2 core and without any shift in 2θ values for Pt. The diameters of the core–shell particle structures, measured using high-resolution transmission electron microscopy images, were in the range of 3–16 nm. The electrochemical profile for SnO_2@Pt/C in an acidic medium (H_2SO_4 at a concentration of 0.5 mol L^{-1}) was almost the same as the typical electrochemical behavior for Pt in an acidic medium. Furthermore, the onset potential for the ethanol oxidation reaction using SnO_2@Pt/C was almost the same as that for PtSn/C E-tek (0.23 V versus the reversible hydrogen electrode). However, the mass current peak densities for ethanol oxidation were 50% higher on SnO_2@Pt/C than on PtSn/C E-tek. In the polarization curve, the mass current density for ethanol oxidation was higher at all potentials for SnO_2@Pt/C when compared to Pt/C and PtSn/C E-tek. At 0.5 V, the current mass density for ethanol oxidation on SnO_2@Pt was 2.3 times of that for the same process on the commercial material. The electrocatalytic activity of SnO_2@Pt/C for ethanol oxidation was associated with an increase in the electrochemically active surface area. However, an electronic effect should also be considered because the Pt shell changes its electronic structure in the presence of the foreign core.

1. Introduction

Direct ethanol fuel cells (DEFCs) have attracted great interest as alternative power sources in the last few years [1–3]. Ethanol is one of the most promising fuels due to its low toxicity, high energy density, and abundant availability as well as the fact that it can be obtained from biomass and produced in many different countries from agricultural products [4–6]. However, the ethanol oxidation reaction (EOR) is a more complicated phenomenon than the methanol oxidation reaction, and it requires more active and selective anode catalysts [7]. Therefore, the exploitation of an effective catalyst with higher EOR activity is a key research objective in the development of DEFCs [2]. In particular, there has been a focus on the cleavage of the C–C bond, which is a pre-condition for the complete oxidation of ethanol to CO_2 [6,7].

Many studies have indicated that PtSn/C is the best electrocatalyst for anodes in a DEFC in comparison with other Pt-based binary catalysts [8,9]. In contrast, insight into the promoting effect of Sn on the activity of the Pt catalyst has been controversial, and discrepant viewpoints have focused on the effects of either alloying Sn into the Pt [3,10,11] or having SnO_2 present [12–15]. SnO_2 is well known for being potentially able to provide O-species for the oxidation of CO produced during the dissociative adsorption of ethanol on Pt active sites (bi-functional mechanism) [3,16,17]. In contrast, the PtSn alloy phase strengthens the electronic effect of the PtSn/C catalyst [3], and DEFCs using Pt_3Sn as the anode catalyst have shown the best average performance in the temperature range of 70–100 °C in comparison with $Pt_{90}Sn_{10}$ and Pt_3Sn E-tek, as reported by Colmati et al. [18]. This phenomenon was probably due to the strengthened electronic effect.

Preparing binary Pt–Sn alloys with a predominant phase, however, is a great challenge [19]. Another way to produce an electronic effect during the electrocatalysis of small organic molecules with a Pt–Sn binary catalyst is through the use of SnO_2@Pt core–shell structures [20]. In the literature, metallic multilayers have been obtained in different systems, and their effects on electrocatalysis of methanol and/or ethanol oxidation have been explained by electronic effects [21–23]. Clearly, a possible core–shell structure could be a metallic bilayer in a nanoparticle system, which is supposed to maintain modifications of "d" band levels, as suggested by Norskov's group [24–26]. In Ru@Pt core–shell structures, evidence has been provided that the main effect of the material must be the

* Corresponding author. Tel.: +55 11 4996 0163; fax: +55 11 4996 0090.
E-mail address: mauro.santos@ufabc.edu.br (M.C. Santos).

0926-3373/$ – see front matter © 2010 Elsevier B.V. All rights reserved.
doi:10.1016/j.apcatb.2010.06.031

result of changes in the electronic structure of the platinum shell [27].

Core–shell materials also present a great advantage for improved Pt utilization in the electrocatalyst [28,29]. Both the Pt amount used is small, and the electrochemical surface area is high when compared to Pt/C with the same load [29,30]. Recently, electrocatalysts in core–shell structures have gained much attention [30–33]. These materials have been prepared by different methods [30,31,33]. Kristian and Wang [30] tested Au@Pt/C core–shell catalysts for their electrocatalytic effects on methanol oxidation. The materials were prepared using successive reductions with an appropriate reducing agent ($NaBH_4$). Using this approach, the authors obtained Au core sizes of 4.8 nm and a complete Pt shell of thickness 0.6 nm. They then demonstrated the improved Pt utilization with these core–shell structures. Chen et al. [32] constructed Au@Pt/C core–shell catalysts from colloidal metallic nanoparticles prepared by adding a reducing agents (tannic acid and trisodium citrate) to solutions containing Au and Pt metal salts at different ratios. With this method, they synthesized nanoparticles with 2-nm diameters. Alayoglu et al. [27] prepared Ru@Pt/C core–shell catalysts by employing Ru nanoparticles in a sequential polyol process. Subsequently, the particles were coated with Pt by adding $PtCl_2$ to the Ru/glycol colloid. The synthesized Ru@Pt nanoparticles showed a mean particle size of 4.1 nm. The authors used these core–shell structures to study CO oxidation on H_2 obtained by reforming hydrocarbons. Using density functional theory, they suggested that the enhanced catalytic activity of the core–shell structures originated from a combination of increased availability of CO-free Pt sites on the Ru@Pt nanoparticles and a hydrogen-mediated, low-temperature CO oxidation process that was distinct from the traditional bi-functional CO oxidation mechanism.

It is clear from the studies described above that the production of a catalyst with a core–shell structure is a good strategy for controlling the reactivity, and consequently, the catalytic activity of the element in the shell. Using such a strategy for the production of a SnO_2@Pt/C catalyst to activate ethanol oxidation in acidic medium can be advantageous even if the recovery of some SnO_2 nanoparticles by Pt is incomplete. In this case, the activation of the ethanol oxidation reaction by the SnO_2 surface-mediated bi-functional mechanism could be beneficial for global catalyst activity.

To our knowledge, a systematic study of the formation of core–shell SnO_2@Pt/C structures with the main goal of obtaining electrocatalysts for the ethanol oxidation reaction has not been published yet. For this reason, we decided to investigate a new and easily employed preparation method to obtain SnO_2@Pt/C structures. In this work, we prepared core–shell SnO_2@Pt/C and Pt/C nanoparticle electrocatalysts by a salt reduction process. The obtained electrocatalysts were tested in ethanol electro-oxidation, and the performances were compared to commercial PtSn/C E-TEK electrocatalysts.

2. Experimental

2.1. Preparation of SnO_2@Pt/C, Pt/C and $PtSnO_2$/C

The electrocatalyst SnO_2@Pt/C in a Pt:Sn atomic ratio of 1:1 was prepared by a new method, which was adapted from methods presented by Kristian and Wang [30] and Braidy et al. [34] to produce Au@Pt, and by Zhang et al. [35] to produce SnO_2 nanoparticles. For the core preparation, $SnCl_2$ (96%, Sigma–Aldrich) was added to water with sodium citrate (Sigma–Aldrich) in the same molar proportion. Subsequently, the solution was vigorously stirred and heated to 90 °C. Then, 21-mmol L^{-1} sodium borohydride (99.9%, Sigma–Aldrich) was added to the $SnCl_2$ solution. The shell was prepared from H_2PtCl_6 (37.5%, Sigma–Aldrich) and ascorbic acid (99%, Sigma–Aldrich) in excess and added to the core solution at 90 °C. In the next stage, carbon Vulcan XC-72R was added to the solution to give a total metal loading of 20 wt%. This step was followed by continuous stirring for 24 h at room temperature. Next, the resulting solution was sonicated for 20 min, and the catalyst then was thermally treated at 300 °C for 1 h under flowing N_2. For comparison, a Pt/C electrocatalyst was prepared (20 wt% metal on carbon XC72R) in the same manner as the Pt shell. By comparing the amount of Pt used to prepare Pt/C and SnO_2@Pt/C, we found that the second had 40% less Pt than the first. At this point, it is important to emphasize that SnO_2@Pt/C had 20% less Pt than that used to prepare Pt_3Sn/C, one of the best binary catalysts for ethanol oxidation [18]. Additionally, in order to make comparisons among the X-ray diffraction patterns and voltammetric responses of the different electrocatalysts, a $PtSnO_2$/C (3:1) electrocatalyst (20 wt% metal on carbon XC72R) was prepared using the sol-gel method [36]. Briefly, in a Vulcan carbon XC72R, adequate amounts of H_2PtCl_6. 7 H_2O and $SnCl_2$ were added in a ratio of 3:1 with PtSn in order to obtain an electrocatalyst with 20% of the metal loading on carbon. Subsequently, appropriate amounts of isopropylic alcohol and acetic acid were added to the mixture. Then, the mixture was homogenized in an ultrasonic bath over 30 min. After 1 h, the mixture was thermally treated at 400 °C for 1 h under flowing N_2.

2.2. Physical characterization

XRD patterns of the catalyst samples were recorded in a Rigaku diffractometer, model Miniflex, using Cu Kα radiation (1.5406 Å, 30 kV and 15 mA). The catalyst morphology and particle size were obtained using JEOL 3010 TEM-HR and JEOL JSM-5900LV microscopes. Measurements of absorption in the visible region were performed in a Varian Cary 50 spectrophotometer.

2.3. Electrochemical measurements

Electrochemical measurements were performed at room temperature (T = 25 °C) using an Autolab PGSTAT 302N potentiostat. The electrodes used were glassy carbon electrodes (support for the working electrodes with a geometric area of 0.2 cm^2) with a Pt counter electrode and a reversible hydrogen electrode as the reference. The glassy carbon (GC) support was polished to a mirror finish with a 1-μm alumina suspension and washed in a mixture of ethanol with water before each experiment. The water used in all experimental procedures was obtained from a Milli-Q system from Millipore®.

The working electrodes were constructed by dispersing 8 mg of electrocatalyst powder in 1 ml of water and mixing for 5 min in an ultrasonic bath. After this procedure, 20 μl of Nafion® solution (5%) was added to the suspension and mixed again in an ultrasonic bath for 15 min. Aliquots of 16 μl of the dispersion fluid were pipetted onto the glassy carbon support surface. Finally, the electrode was dried at 60 °C for 20 min and hydrated for 5 min in water. The cyclic voltammetric, chronoamperometric and polarization experiments were performed in a 0.5-mol L^{-1} H_2SO_4 solution in both the absence and presence of a 0.5-mol L^{-1} solution of ethanol. The electrochemical cell was purged for 15 min with N_2 before each experiment.

3. Results and discussion

3.1. Physical characterization

The UV–vis absorption spectrum of SnO_2@Pt nanoparticles is presented in Fig. 1, where platinum and tin oxide are also presented

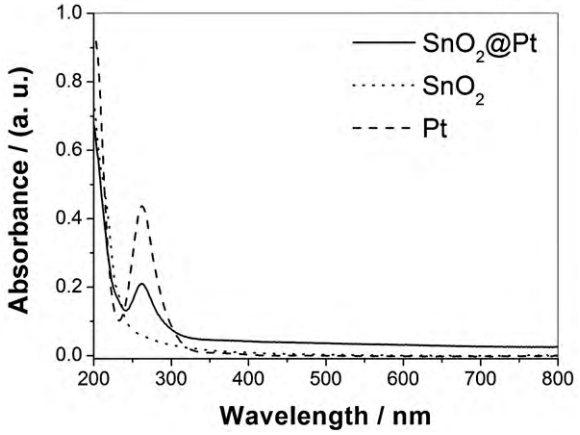

Fig. 1. UV–vis absorption spectra of SnO_2, Pt and SnO_2@Pt nanoparticles.

for comparison. Although the composition of the core just after its preparation is difficult to characterize only by UV measurements, the analysis of the results obtained with this technique for the core indicate that a mixture of different compounds is produced at the end of this process. Further, when the core–shell structure is formed, the core is composed of SnO_2. Thus, Sn^{2+} was reduced to Sn^0, which was gradually converted to SnO_2, onto which the Pt nanoparticles were subsequently deposited. The formation of SnO_2 is supported by the results of additional techniques, as will be presented later in the following sections. The formation of Sn^0 nanoparticles can be observed by UV–vis measurements, but the presence of adsorption bands that are typical for this element in the UV spectrum depend on the physicochemical properties and composition of the medium in which the particles are contained, as reported by Melendrez et al. [37]. None of the UV spectra presented in reference [37] are similar to the spectrum obtained for the core in Fig. 1, but there are no similarities in the experimental conditions for the cases studied in this reference when compared with the experimental conditions of this work. Additionally, the influence of tin oxides (SnO, SnO_2 or both) in the UV signal of Sn^0 was not considered. Tin-based nanoparticles composed only of oxidized species such as SnO_2 have typical band gap values ranging from 4.0 to 4.6 eV [38], which are higher than the values for the bulk materials (3.6 eV for SnO_2) because of quantum confinement effects [38]. When SnO_2 was present at the surface, the onset of the absorption in the UV region could be used to estimate the band gap. Using such an approach, the value of 4.9 eV was obtained, which is far from the expected value of pure SnO_2 nanoparticles or even for a mixture of SnO and SnO_2 [39]. The procedure used above for the calculation of the band gap is valid only for samples containing SnO or SnO_2. The deviation from the expected value observed is probably due to the presence of Sn^0. It is important to note that Sn@Pt/C could also be an interesting catalyst for ethanol electro-oxidation. However, a catalyst in such a configuration is not easily obtained. Tin is a very reactive element, and in the experimental conditions used in the present work, the existence of Sn in the metallic state was possible only for a short amount of time. To increase the dwell time of

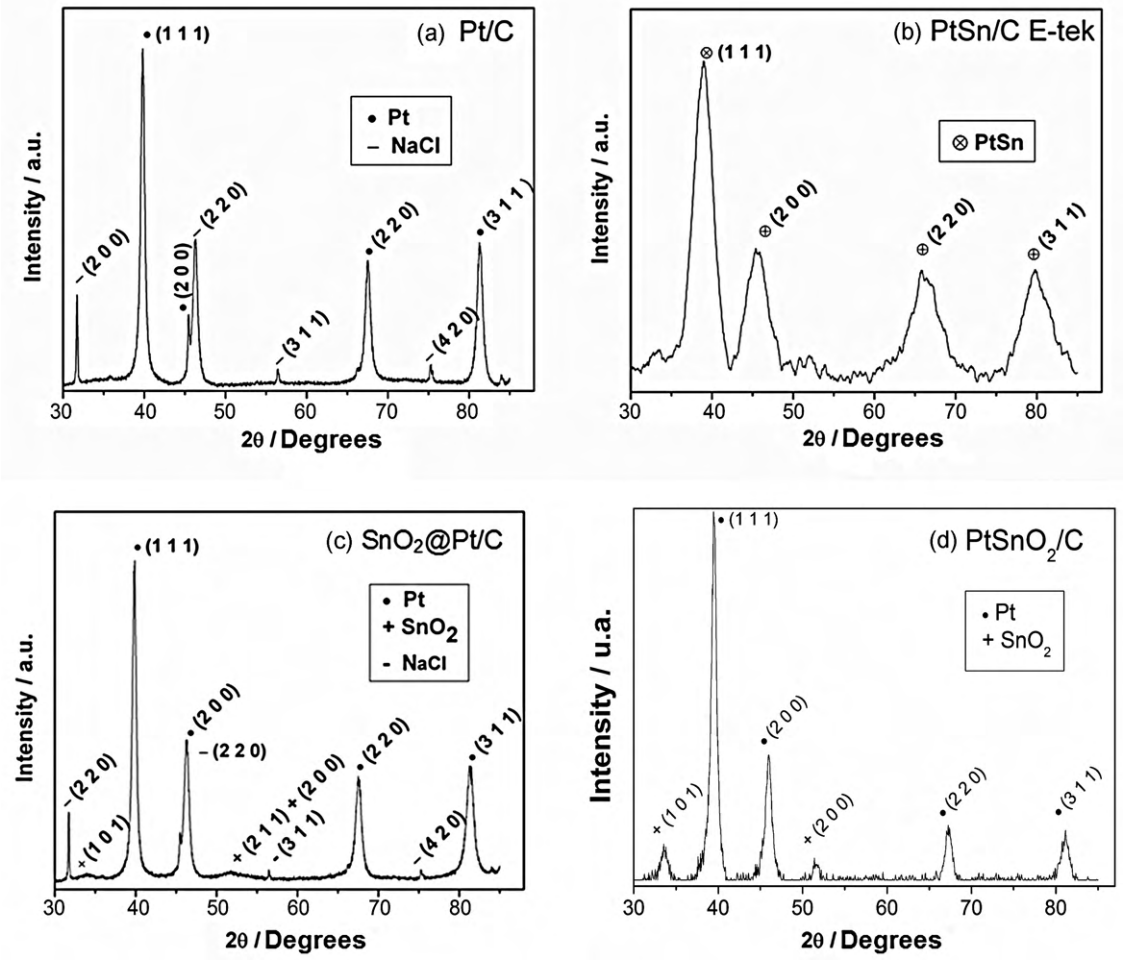

Fig. 2. X-ray diffraction patterns of (a) Pt/C, b) PtSn/C E-Tek, (c) SnO_2@Pt and (d) $PtSnO_2$/C electrocatalysts.

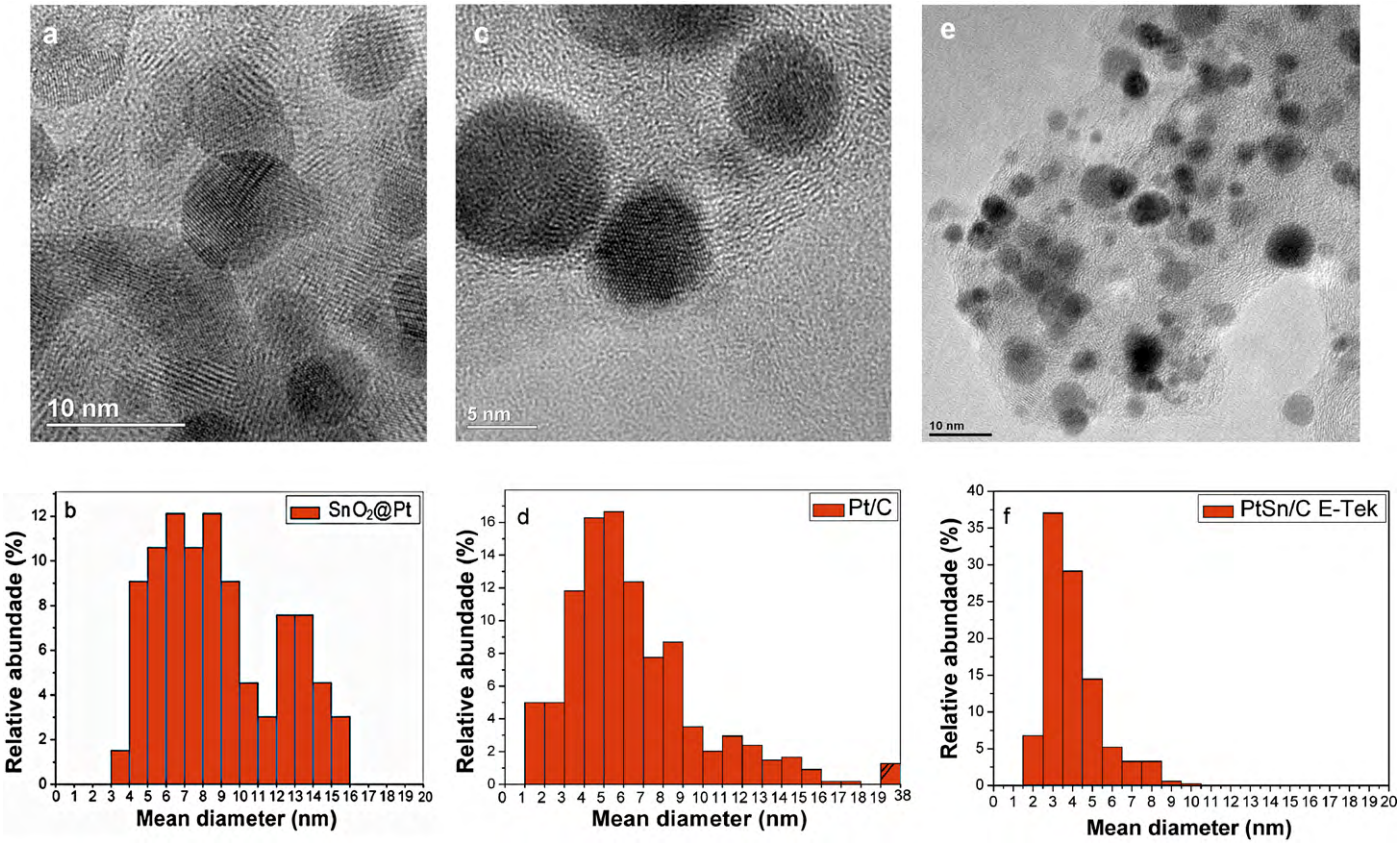

Fig. 3. (a) TEM micrograph of the SnO_2@Pt/C electrocatalyst; (b) histogram of the catalyst particle mean diameter distribution over a size range of 0–16 nm; (c) TEM micrograph of the Pt/C electrocatalyst; (d) histogram of the catalyst particle mean diameter distribution over the size range of 0–38 nm; (e) TEM micrograph of the PtSn/C E-tek electrocatalyst; (f) histogram of the catalyst particle mean diameter distribution over the size range of 0–10 nm.

metallic Sn, either the tin nanoparticles formed must be protected or other methodology must be used to ensure that the oxidation of the surface does not occur. Additionally, Sn@Pt nanoparticles would be adequate catalysts for ethanol electro-oxidation in acidic environments only if the Pt shell is complete. If the shell is not complete, the core could be dissolved by the formation of SnO.

For Pt, an absorption peak at 262 nm due to the surface plasmon resonance of Pt nanoparticles was clearly observed [13]. The same feature was also observed for SnO_2@Pt nanoparticles. In this case, however, a much lower intensity indicated that the Pt nanoparticles were formed in lower amounts than in the case of Pt alone. The obtained results also suggested that there was no alloy formation between Pt and Sn, which was confirmed by XRD measurements. When Pt was alloyed with Sn, the plasmon resonance of Pt nanoparticles at 262 nm vanished, as previously demonstrated by Zheng et al. [13]. These results strongly suggest the formation of a core–shell structure in these nanoparticles.

Fig. 2 shows XRD diffraction patterns of the nanomaterials prepared from Pt/C and SnO_2@Pt/C and, for comparison, PtSn/C E-Tek and $PtSnO_2$/C nanoparticles. Pt/C, SnO_2@Pt/C and $PtSnO_2$/C presented characteristic (1 1 1), (2 0 0) and (2 2 2) Pt diffraction peaks observed at $2\theta = 39.800^\circ$, 46.200°, and 67.460°, respectively. These results were in good agreement with the Pt standard (JCPDS PDF#04-0802) without any shift in 2θ, which further indicated the absence of alloy formation between Pt and Sn and the presence of segregated Pt and SnO_2 phases in $PtSnO_2$/C. Other peaks were present for Pt/C and SnO_2@Pt/C, which were related to the NaCl (JCPDS PDF#77-6024) that originated from the preparation process. For SnO_2@Pt/C, it was possible to observe very small peaks for SnO_2 ($2\theta = 34^\circ$ and 51.8°) that were almost at the same level as the noise. These facts demonstrate that the initially formed Sn nanoparticles were subsequently converted to SnO_2. Furthermore, it was clear from the results that Pt was deposited on the SnO_2 core without the formation of an alloy between Pt and Sn or in the segregated phases of Pt and SnO_2. On the other hand, PtSn/C E-tek electrocatalysts presented typical diffraction peak patterns of a PtSn alloy (JCPDS PDF#25-614). Further, $PtSnO_2$/C, for which even Pt was observed in greater amount than Sn (ratio 3:1), had a SnO_2 phase with considerable peak pattern intensities ($2\theta = 34^\circ$ and 51.8°).

The HRTEM images and histograms of the electrocatalysts SnO_2@Pt/C, Pt/C and PtSn/C E-tek are shown in Fig. 3a–f. In these figures, the morphology and particle size distribution can be seen. Based on the data in the figures, all electrocatalysts were well distributed on the carbon support, and the particle sizes were between 3 and 16 nm for 100% of the particles in SnO_2@Pt/C (see Fig. 3a and b). For Pt/C, 99% of the particle sizes were between 1 and 16 nm (see Fig. 3c and d). All PtSn/C E-Tek particle sizes were smaller than 10 nm (see Fig. 3e and f), in agreement with the work of Colmati et al. [18].

3.2. Electrochemical experiments

Fig. 4 displays the cyclic voltammetry results for the electrocatalysts in an acidic medium (H_2SO_4 at a concentration of 0.5 mol L^{-1}): (a) SnO_2@Pt/C, (b) Pt/C, (c) PtSn/C E-Tek and (d) $PtSnO_2$/C. For the SnO_2@Pt/C electrocatalyst, it was possible to observe a very similar electrochemical profile when comparing both the Pt/C prepared here and the Pt/C that has been extensively described in the literature [7,40–42]. Briefly, there were well-defined processes associated with the adsorption/desorption of hydrogen on Pt between 0.05 and 0.4 V. For PtSn/C E-Tek, this region was not

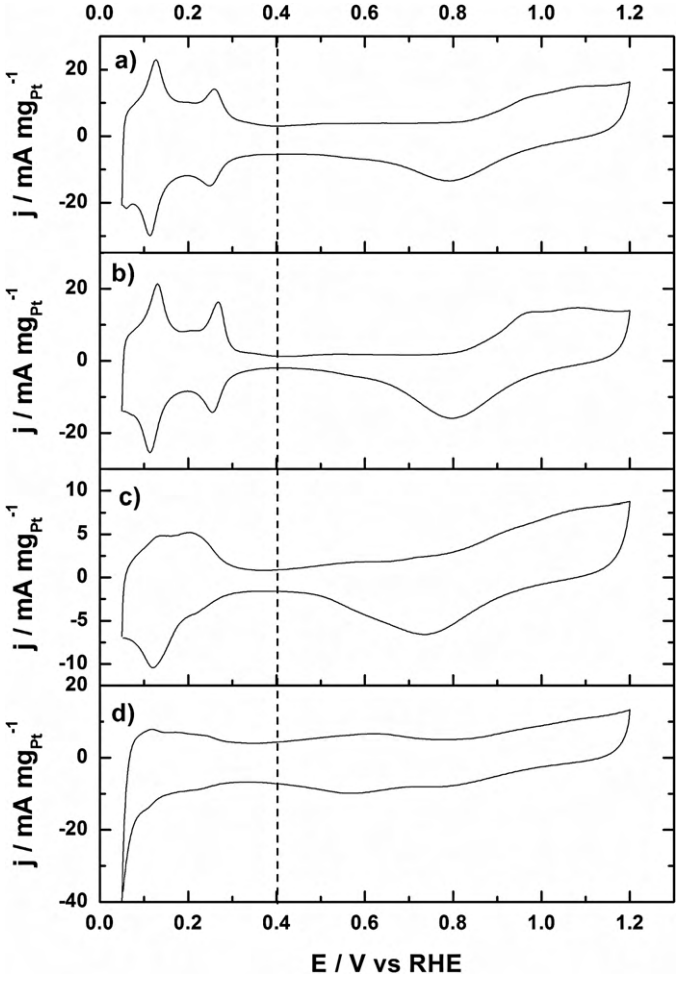

Fig. 4. Cyclic voltammograms of a) SnO_2@Pt/C, b) Pt/C, c) PtSn/C E-Tek and d) $PtSnO_2$/C in 0.5-mol L^{-1} H_2SO_4 aqueous solutions at a potential sweep rate of 50 mV s^{-1}. T = 25 °C.

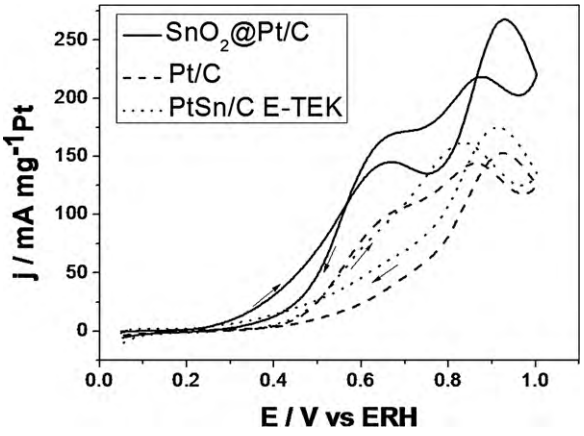

Fig. 5. Cyclic voltammograms of SnO_2@Pt/C, Pt/C and PtSn/C E-Tek in 1.0-mol L^{-1} CH_3CH_2OH + 0.5-mol L^{-1} H_2SO_4 aqueous solutions at a potential sweep rate of 10 mV s^{-1}. T = 25 °C.

well defined because of the presence of tin, as demonstrated by Kim et al. [11]. In the double layer region of SnO_2@Pt/C, between 0.4 and 0.85 V, a larger capacitive current was observed than with Pt/C or PtSn/C E-tek. This effect could have been due to exposure of the SnO_2 core from pinholes on the incomplete Pt shell of some of the particles. These anomalies have already been suggested to be the result of incomplete formation of Pt monolayer shells on the core by Alayoglu et al. [27] for Ru@Pt core–shell structures. On the other hand, the voltammetric profile for PtSn/C E-tek showed an influence of tin in all potential regions, including a strong shape difference in the hydrogen adsorption/desorption on the PtSn/C alloy [11]. Additionally, the formation and reduction of PtO occurred in the same region of the potentials for SnO_2@Pt/C and Pt/C. It is important to stress that for the $PtSnO_2$/C electrocatalyst, in which Pt and SnO_2 nanoparticles are segregated as demonstrated in the X-ray diffraction patterns, the cyclic voltammetric response of the surface is completely different than the one related to SnO_2@Pt/C. The voltammetric profile for $PtSnO_2$/C presents a hydrogen adsorption and desorption potential region between 0.05 and 0.4 V that was inhibited by the presence of SnO_2 in the electrocatalyst. Moreover, the cyclic voltammogram curve of the $PtSnO_2$/C catalysts shows an increase in the current density at the double layer between 0.4 and 0.8 V, which could be related to Sn oxide species segregation. The peaks that appeared around 0.66 and 0.60 V may be attributed to the O_2 adsorption/desorption from the dissociation of water onto Sn oxide [15]. Pt segregated PtO between 0.8 and 1.2 V and the reduction of this oxide occurred at 0.8 V. By comparing SnO_2@Pt/C and $PtSnO_2$/C electrocatalysts, if the Pt of the material SnO_2@Pt/C was nucleated in a great amount of Pt dispersed in the electrocatalyst, the voltammetric profile for this material would be very similar to the one associated to $PtSnO_2$/C. This fact highlights the formation of the SnO_2@Pt/C structure.

These voltammetric characterizations, combined with UV–vis spectra and XRD patterns for SnO_2@Pt/C electrocatalysts, suggested the definite formation of the core–shell structure.

The cyclic voltammetric features for ethanol oxidation on SnO_2@Pt/C, Pt/C and PtSn E-Tek electrocatalysts are presented in Fig. 5. Oxidation currents for the ethanol oxidation process were observed during both forward and backward scans. The onset potentials obtained for the different catalysts studied were 0.23 V for SnO_2@Pt/C, 0.37 V for Pt/C and 0.23 V for PtSn/C E-Tek. The value of the onset potential for ethanol oxidation commonly found for Pt/C in the literature is 0.37 V [43], but this value is highly affected by the incorporation of tin in the catalyst. The lowest onset potential obtained for the ethanol oxidation process using PtSn/C E-Tek could be explained by the presence of Sn, which might promote ethanol oxidation through either an electronic effect and/or a bi-functional effect in the Pt-based material, decreasing the overall activation energy for the EOR [44–46]. In the core–shell structure, SnO_2 was present on the electrocatalyst surface only for a small portion of particles because of the exposure of the core from pinholes in incomplete Pt shells. Thus, the produced electrocatalyst effect was likely associated with an electronic effect caused by a modification of the "d" band level, as proposed by researchers using metallic bilayers [21–23] and core–shell structures [26]. The influence of the tin oxide exposed in some defective Pt shell layers was possible for a bi-functional mechanism [8], but it was difficult to pin down precisely in which step the reaction mechanism was affected.

The mass current densities for ethanol oxidation on SnO_2@Pt/C in Fig. 5 were all higher than the ones for the same process using Pt/C or PtSn/C E-tek as the electrocatalysts. There are three synergic possible reasons for these results: (i) an increase in the Pt surface area [27,30,47]; (ii) a change in the "d" band level of the material [19,21–23], which might be related to a more efficient intermediate oxidation and/or a decrease in poisoning by strongly bound species generated during the ethanol oxidation [3,12,16]; or (iii) the removal of adsorbed intermediates by a bi-functional mechanism, which was promoted by the SnO_2 exposed by pinholes in the incomplete Pt shell. Additionally, a change in the oxidation mechanism for the EOR using SnO_2@Pt as an electrocatalyst instead of Pt/C and PtSn/C E-tek may be possible.

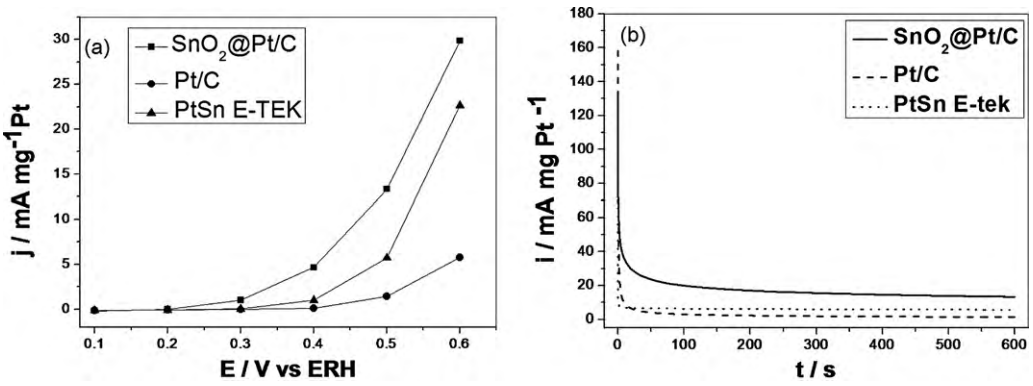

Fig. 6. (a) Polarization curves for the 20 wt% electrocatalyst on carbon in 1.0-mol L^{-1} CH_3CH_2OH + 0.5-mol L^{-1} H_2SO_4, t = 10 min per point; (b) Chronoamperometry curves for $E_{oxidation}$ = 0.5 V and t = 10 min.

Fig. 6a and b shows the chronoamperometry and polarization curve studies for ethanol electro-oxidation by the different electrocatalysts studied. The results corroborate the cyclic voltammetric experiments and indicate that the electrocatalyst SnO_2@Pt/C displayed a mass current density for ethanol oxidation that was 2.3 times greater than PtSn/C E-Tek at 0.5 V. Furthermore, SnO_2@Pt/C had higher current densities in all potentials in the polarization curve. Again, as discussed for cyclic voltammetric experiments, an increase in the Pt surface area [27,30,47] or a change in the "d" band level of the material could be suggested as possible explanations for the enhancement of the electrocatalytic activity in ethanol oxidation.

At this point, it is important to stress the different advantages of the SnO_2@Pt system: (i) it is capable of modifying the electronic properties of Pt; (ii) by using this material, there is a decrease in the amount of Pt on the electrocatalyst, which reduces cost; and (iii) it presents electrocatalytic activity toward ethanol oxidation that is better than PtSn/C E-tek commercial electrocatalysts. These advantages suggest that SnO_2@Pt/C could be a promising material for direct ethanol fuel cells.

4. Conclusions

A new core–shell material for the ethanol oxidation reaction, SnO_2@Pt/C, was prepared by a novel route. Its formation was confirmed by UV–vis spectra, XRD and electrochemical methods. Using high-resolution transmission electron microscopy, it was possible to measure the particle sizes in the range of 3–16 nm. Using voltammetric experiments, polarization curves and chronoamperometric experiments, the SnO_2@Pt/C structure showed a good enhancement of electrocatalytic activity toward ethanol oxidation compared to Pt/C and PtSn/E-tek. The results using SnO_2@Pt as an electrocatalyst for ethanol oxidation showed that it was possible to improve the use of Pt in electrocatalysis, diminishing the amount of Pt required in the electrocatalyst in the studied case by 40% relative to Pt/C and 20% relative to Pt_3Sn/C. Furthermore, the effect of this material on ethanol oxidation could likely be explained by an increase in the electrochemical surface area and/or a change in the "d" band level, as suggested for bimetallic layers and core–shell structures studied in the literature. The results presented here indicate that SnO_2@Pt/C might be a very promising material in direct ethanol fuel cells.

Acknowledgments

The authors wish to thank the Brazilian funding institutions CNPq (process number: 474732/2008-8), CAPES, FAPESP (processes numbers: 05/59992-6, 09/09145-6, 08/58788-4) and UFABC for their financial support. ETN and JCMS thank LME-LNLS for the use of the JEOL JSM-5900LV microscope and TEM image acquisition. In addition, the authors thank Vera Constantino for the use of the XRD instrument.

References

[1] W.J. Zhou, S.Q. Song, W.Z. Li, G.Q. Sun, Q. Xin, S. Kontou, K. Poulianitis, P. Tsiakaras, Solid State Ionics 175 (2004) 797–803.
[2] M.Y. Zhu, G.Q. Sun, S.Y. Yan, H.Q. Li, Q. Xin, Energy Fuels 23 (2009) 403–407.
[3] M. Zhu, G. Sun, Q. Xin, Electrochim. Acta 54 (2009) 1511–1518.
[4] R.N. Singh, A. Singh, Anindita, Carbon 47 (2009) 271–278.
[5] E. Ribadeneira, B.A. Hoyos, J. Power Sources 180 (2008) 238–242.
[6] A. Kowal, M. Li, M. Shao, K. Sasaki, M.B. Vukmirovic, J. Zhang, N.S. Marinkovic, P. Liu, A.I. Frenkel, R.R. Adzic, Nat. Mater. 8 (2009) 325–330.
[7] R.F.B. De Souza, A.E.A. Flausino, D.C. Rascio, R.T.S. Oliveira, E.T. Neto, M.L. Calegaro, M.C. Santos, Appl. Catal. B 91 (2009) 516–523.
[8] E. Antolini, J. Power Sources 170 (2007) 1–12.
[9] W. Zhou, Z. Zhou, S. Song, W. Li, G. Sun, P. Tsiakaras, Q. Xin, Appl. Catal. B 46 (2003) 273–285.
[10] F. Colmati, E. Antolini, E.R. Gonzalez, Appl. Catal. B 73 (2007) 106–115.
[11] J.H. Kim, S.M. Choi, S.H. Nam, M.H. Seo, S.H. Choi, W.B. Kim, Appl. Catal. B 82 (2008) 89–102.
[12] F.L.S. Purgato, P. Olivi, J.M. Léger, A.R. de Andrade, G. Tremiliosi-Filho, E.R. Gonzalez, C. Lamy, K.B. Kokoh, J. Electroanal. Chem. 628 (2009) 81–89.
[13] L. Zheng, L. Xiong, J. Sun, J. Li, S. Yang, J. Xia, Catal. Commun. 9 (2008) 624–629.
[14] Z. Liu, L. Hong, S.W. Tay, Mater. Chem. Phys. 105 (2007) 222–228.
[15] D.-H. Lim, D.-H. Choi, W.-D. Lee, H.-I. Lee, Appl. Catal. B 89 (2009) 484–493.
[16] M. Zhu, G. Sun, H. Li, L. Cao, Q. Xin, Chin. J. Catal. 29 (2008) 765–770.
[17] R.F.B. De Souza, L.S. Parreira, D.C. Rascio, J.C.M. Silva, E. Teixeira-Neto, M.L. Calegaro, E.V. Spinace, A.O. Neto, M.C. Santos, J. Power Sources 195 (2010) 1589–1593.
[18] F. Colmati, E. Antolini, E.R. Gonzalez, J. Electrochem. Soc. 154 (2007) B39–B47.
[19] R.F.B. De Souza, L.S. Parreira, D.C. Rascio, J.C.M. Silva, E.T. Neto, M.L. Calegaro, E.V. Spinace, A.O. Neto, M.C. Santos, J. Power Sources 195 (2010) 1589–1593.
[20] J. Luo, L. Han, N.N. Kariuki, L.Y. Wang, D. Mott, C.J. Zhong, T. He, Chem. Mater. 17 (2005) 5282–5290.
[21] R.T.S. Oliveira, M.C. Santos, B.G. Marcussi, S.T. Tanimoto, L.O.S. Bulhões, E.C. Pereira, J. Power Sources 157 (2006) 212–216.
[22] R.T.S. Oliveira, M.C. Santos, B.G. Marcussi, P.A.P. Nascente, L.O.S. Bulhões, E.C. Pereira, J. Electroanal. Chem. 575 (2005) 177–182.
[23] R.G. Freitas, E.P. Antunes, E.C. Pereira, Electrochim. Acta 54 (2009) 1999–2003.
[24] E. Christoffersen, P. Liu, A. Ruban, H.L. Skriver, J.K. Norskov, J. Catal. 199 (2001) 123–131.
[25] M.O. Pedersen, S. Helveg, A. Ruban, I. Stensgaard, E. Laegsgaard, J.K. Norskov, F. Besenbacher, Surf. Sci. 426 (1999) 395–409.
[26] K.W. Jacobsen, P. Stoltze, J.K. Norskov, Surf. Sci. 366 (1996) 394–402.
[27] S. Alayoglu, A.U. Nilekar, M. Mavrikakis, B. Eichhorn, Nat. Mater. 7 (2008) 333–338.
[28] Z.D. Wei, Y.C. Feng, L. Li, M.J. Liao, Y. Fu, C.X. Sun, Z.G. Shao, P.K. Shen, J. Power Sources 180 (2008) 84–91.
[29] Y.-N. Wu, S.-J. Liao, Z.-X. Liang, L.-J. Yang, R.-F. Wang, J. Power Sources 194 (2009) 805–810.
[30] N. Kristian, X. Wang, Electrochem. Commun. 10 (2008) 12–15.
[31] M.H. Lee, J.S. Do, J. Power Sources 188 (2009) 353–358.
[32] H.M. Chen, H.C. Peng, R.S. Liu, S.F. Hu, L.Y. Jang, Chem. Phys. Lett. 420 (2006) 484–488.
[33] H. Wang, C. Xu, F. Cheng, M. Zhang, S. Wang, S.P. Jiang, Electrochem. Commun. 10 (2008) 1575–1578.
[34] N. Braidy, G.R. Purdy, G.A. Botton, Acta Mater. 56 (2008) 5972–5983.
[35] H. Zhang, N. Du, B. Chen, T. Cui, D. Yang, Mater. Res. Bull. 43 (2008) 3164–3170.

[36] M.C. Santos, L. Cogo, S.T. Tanimoto, M.L. Calegaro, L.O.S. Bulhões, Appl. Surf. Sci. 253 (2006) 1817–1822.
[37] M. Melendrez, G. Cardenas, J. Diaz, C. Cruzat, J. Arbiol, Colloid Polym. Sci. 287 (2009) 13–22.
[38] A. Muthuvinayagam, N. Melikechi, P.D. Christy, P. Sagayaraj, Phys. B: Condens. Matter 405 (2010) 1067–1070.
[39] H.M. Deng, J.M. Hossenlopp, J. Phys. Chem. B 109 (2005) 66–73.
[40] J.-G. Oh, C.-H. Lee, H. Kim, Electrochem. Commun. 9 (2007) 2629–2632.
[41] Y. Liu, S. Mitsushima, K.-i. Ota, N. Kamiya, Electrochim. Acta 51 (2006) 6503–6509.
[42] E.V. Spinacé, A.O. Neto, T.R.R. Vasconcelos, M. Linardi, J. Power Sources 137 (2004) 17–23.
[43] H. Wang, Z. Jusys, R.J. Behm, J. Power Sources 154 (2006) 351–359.
[44] F.C. Simões, D.M. dos Anjos, F. Vigier, J.M. Léger, F. Hahn, C. Coutanceau, E.R. Gonzalez, G. Tremiliosi-Filho, A.R. de Andrade, P. Olivi, K.B. Kokoh, J. Power Sources 167 (2007) 1–10.
[45] E.A. Batista, G.R.P. Malpass, A.J. Motheo, T. Iwasita, J. Electroanal. Chem. 571 (2004) 273–282.
[46] J.M. Léger, Electrochim. Acta 50 (2005) 3123–3129.
[47] K. Shimizu, I. Francis Cheng, C.M. Wai, Electrochem. Commun. 11 (2009) 691–694.